Combined physical and pharmaceutical anabolic osteoporosis therapies synergistically increase bone response and local mechanoregulation

Authors: Friederike A. Schulte[1†], Julia K. Griesbach[1†], Claudia Weigt, Marcella von Salis-Soglio[1], Floor M. Lambers[1], Francisco C. Marques[1], Michaela Kneissel[3], Peter J. Richards[2,3], Gisela A. Kuhn[1], Ralph Müller[1]*

Affiliations:

[1]Institute for Biomechanics, ETH Zurich; Zurich, Switzerland.
[2]Bone and Stem Cell Research Group, CABMM, University of Zurich; Zurich, Switzerland.
[3]Musculoskeletal Disease Area, Novartis Institutes for Biomedical Research; Basel, Switzerland.

[*]Corresponding author. Email: ram@ethz.ch
[†]These authors contributed equally to this work.

One Sentence Summary:

Combined physical and pharmaceutical anabolic therapies synergistically increase the bone response and local mechanoregulation in osteoporotic mice.

Abstract: Bone loss in postmenopausal osteoporosis is caused by an imbalance between bone formation and resorption in the remodeling process. Existing pharmaceutical therapies act on the cellular mechanisms that allow bone to adapt to mechanical demands by a process called mechanoregulation. This process ensures at the tissue level that bone is formed where needed and resorbed where redundant. Here, we report the effects of combining pharmaceutical therapies, both anti-catabolic and anabolic, with mechanical loading in a mouse model of osteoporosis. Ovariectomized mice were treated with bisphosphonates, parathyroid hormone, sclerostin antibodies, or no treatment (vehicle) for a period of four weeks. At the same time, their sixth caudal vertebrae were subjected to cyclic mechanical or sham loading. Bi-weekly time-lapsed *in vivo* micro-computed tomography revealed that mechanical loading synergistically enhanced the increase in trabecular bone response to anabolic, but not to anti-catabolic, osteoporosis treatments. Comparing bone formation and resorption volumes to the underlying mechanical environment demonstrated that all treatments showed higher strain values in regions preceding bone formation and lower strain values in regions preceding bone resorption. Compared to vehicle, higher mechanoregulation was found in anabolic, and lower mechanoregulation in anti-catabolic treatments. However, combining anabolic and physical treatments synergistically increased mechanoregulation, indicating that mechanical loading amplifies the effectiveness of anabolic therapies by driving bone (re)modeling to better align with the bone's mechanical demands. These findings suggest that incorporating load-bearing physical therapy into anabolic pharmaceutical treatment regimens holds promise for enhancing therapeutic outcomes in osteoporosis management.

INTRODUCTION

Osteoporosis is a prevalent disease characterized by reduced bone mass and structural deterioration of bone tissue, leading to increased bone fragility and susceptibility to fractures (*1*). As a major public health concern, osteoporosis primarily affects the elderly, particularly postmenopausal women, although men are also at risk. The pathogenesis of osteoporosis involves an imbalance between bone resorption by osteoclasts and bone formation by osteoblasts. The mechanisms underlying osteoporosis are multifaceted and include hormonal changes, particularly the decline in estrogen levels in postmenopausal women, genetic predispositions (*2*), nutritional deficiencies (*3*), and lifestyle factors such as physical inactivity and smoking (*4*). Understanding these mechanisms has been critical in developing pharmaceutical therapies aimed at preventing and treating osteoporosis. Several pharmaceutical agents are currently available for the management of osteoporosis, each targeting different aspects of bone metabolism. Bisphosphonates are the most widely prescribed class of drugs for osteoporosis. These compounds, such as alendronate and zoledronate, inhibit osteoclast-mediated bone resorption by binding to hydroxyapatite crystals in bone, thereby preventing osteoclast attachment and activity. This anti-catabolic action helps to maintain bone density and reduce the risk of fractures (*5*). Parathyroid hormone analogs, such as teriparatide, are an anabolic therapeutic option. These agents stimulate bone formation by activating osteoblasts. Teriparatide, a recombinant form of parathyroid hormone, is used for severe osteoporosis and has been shown to significantly increase bone mineral density and reduce the risk of fractures (*6*). Humanized monoclonal antibodies, such as sclerostin antibodies, represent another anabolic approach to osteoporosis treatment. Sclerostin antibodies target sclerostin, a protein that inhibits the Wnt-signaling pathway, which is crucial for bone formation (*7*). By binding to and inhibiting sclerostin, sclerostin antibodies promote osteoblast activity and bone formation while also reducing bone resorption (*8*). Clinical trials have demonstrated that sclerostin antibodies significantly increase bone mineral density and reduce the risk of vertebral and non-vertebral fractures (*9*). Interestingly, the Wnt-signaling pathway is also activated during supraphysiological mechanical loading. Supraphysiological mechanical loading in the form of physical therapy has also been reported to have positive effects on the risk reduction of major osteoporotic fractures (*10*).

In fact, next to responding to pharmaceutical treatments, bone has been known for its ability to functionally adapt to mechanical demands: highly loaded bones increase their density while disused bones decrease it, a concept referred to as mechanostat (*11*). In the trabecular compartment in particular, the incoming demands are transferred to the tissue level where osteocytes perceive local mechanical signals and translate them into bone formation by osteoblasts and resorption by osteoclasts. The resulting adaptation of form is called (anabolic or catabolic) bone modeling and (spatially coupled) bone remodeling, collectively referred to as bone (re)modeling. Large portions of the bone (re)modeling can be attributed to mechanoregulation, the concept of regional orchestration of formation and resorption activity according to local mechanical stimuli (*12-15*). Portions of site-unspecific non-targeted bone (re)modeling occur, which are related to maintaining mineral homeostasis (*16, 17*). It has been shown that supraphysiological mechanical loading decreases the non-targeted portions of bone remodeling by increasing the sensitivity of mechanoregulation mechanisms which ensure that induced bone gain is more targeted to the mechanical needs of the bone (*18, 19*).

An open research question is whether osteoporosis patients under treatment may increase therapy outcome by additional physical treatment. Physical and pharmaceutical therapies could be easily combined in individual treatment plans. Previously, however, mechanical loading did not interfere with bisphosphonate treatment, neither in trabecular nor in cortical regions of tibias in C57BL/6 mice (*20*). In contrast, mechanical loading combined with intermittent PTH (1-34) at 80 μg/kg/day led to synergistic effects in cortical but not trabecular bone volume of the

proximal tibia and distal ulna in 13-17-week-old healthy mice (*21*). The authors reported that the missing trabecular synergistic effects of loading might have been obscured by the dramatic dose-related effects that PTH alone had on trabecular bone. In 19-month-old healthy mice, additive benefits in the periosteal cortical regions of the tibia were reported at 50 µg/kg/day intermittent PTH while in the trabecular bone the loading-related increase in bone volume fraction (BV/TV) was abrogated (*22*). Mechanical loading combined with sclerostin antibodies in healthy young mice led to a synergistic increase in cortical but not trabecular bone volume and thickness (*23*). Robinson et al. (*26*) reported synergistic effects in the trabecular compartment of the healthy tibia, but only prevalent in regions that were not remodeled but modeled (*24*). While effects of pharmaceutical treatments and their combination with mechanical loading on trabecular bone have been controversially discussed, treatment effects on mechanoregulation in trabecular bone remain completely unclear. Assessing if the morphometric effects resulting from pharmaceutical treatments are targeted to mechanical demands would help understand treatment efficacy in fracture prevention. The aims of the current study were to investigate to which extent I) pharmaceutical treatments target bone (re)modeling to the places that mechanically need it, II) their combination with mechanical loading improves the treatment effect, and III) pharmaceutical treatments or their combination with mechanical loading lead to increased mechanoregulation.

To address these aims, we administered bisphosphonate (BIS), parathyroid hormone (PTH), sclerostin antibody (SclAB) or vehicle (VEH) treatment to ovariectomized 20-week-old C57BL/6 mice. Regional mechanical loading (ML) was applied through a highly controlled vertebra loading model that has been shown to induce a 20% increase BV/TV in trabecular bone in healthy mice (*25*). In short, cyclic mechanical stimulation was applied to the 6th caudal vertebra through a mechanical loading device using stainless steel pins in the adjacent vertebrae. *In vivo* time-lapsed micro-computed tomography (micro-CT) allowed assessment of bone formation and resorption volumes, and micro-finite-element-(FE)-modeling was used to determine the mechanical environment. All treatments targeted bone (re)modeling to the places that mechanically needed it. We found synergistic effects with mechanical loading in the trabecular bone response in anabolic but not in anti-catabolic treatments. Differences in the sensitivity of mechanoregulation mechanisms in the bone response were identified, which may help understand synergisms when combining mechanical loading with anabolic osteoporosis therapies. These findings highlight the potential of physical therapy as an adjunct to pharmaceutical anabolic treatment towards fracture risk reduction and an improved management of postmenopausal osteoporosis.

RESULTS

Monotreatments increase bone volume via differing (re)modeling mechanisms

C57BL/6 mice were ovariectomized at 15 weeks-of-age. All animals (n=105) lost BV/TV in response to ovariectomy as verified by micro-CT of the 6th caudal vertebra (-26.8±9.7% change in BV/TV compared to start of treatment, data presented as mean ± standard deviation). From week 20 to 24, animals received pharmaceutical treatment and/or mechanical loading (Fig 1A). The VEH-group showed a further decrease in BV/TV between weeks 20 and 24 (-10.1±7.6%, Fig 1B). In all monotreatment groups including the ML-group, BV/TV increased (ML: 17.7±11.0%; BIS: 14.4±8.5%; PTH: 22.1±10.0%; SclAB: 25.3±12.7%; Fig 1B). The BIS-group showed no significant increase in trabecular thickness (Tb.Th: 4.8±4.0%) compared to the VEH-group (0.5±4.4%). The anabolic treatment groups increased in Tb.Th with the increase in the PTH-group being significantly less pronounced than the other anabolic treatment groups (ML: 20.6±8.3%, PTH: 11.6±4.7%, SclAB: 25.3±6.9%; Fig 1C). Trabecular number (Tb.N) was preserved in the BIS-group (1.1±2.9%), and decreased in all other groups (VEH: -

8.8±4.0%; ML: -8.1±3.4%; PTH: -6.3±2.9%; SclAB:-10.4±2.7%; Fig 1D). Connectivity density (Conn.D) remained intact in the BIS-group (1.1±15.3%) and decreased in all other groups, where the loss of Conn.D in the PTH-group was significantly less than in ML and SclAB (VEH: -21.2±11.2%; ML: -29.5±12.9%; PTH: -6.4±20.5%; SclAB: -35.0±8.3%; Fig 1E).

Fig 1F shows bone formation and resorption volumes evolving over time. Bone formation rate (BFR) in week 22 to 24 in the BIS-group (BIS: 1.0±0.2%/d) was lower than in the PTH- and SclAB-group (PTH: 1.5±0.3%/d, SclAB: 1.6±0.3%/d, Fig 1G). VEH and ML showed no significant differences to the other groups (VEH: 1.3±0.5%/d; ML: 1.4±0.3%/d). Mineral apposition rate (MAR) did not differ significantly amongst groups (Fig 1H). Mineralizing surface (MS) was higher in the anabolic groups (ML: 56.5±6.8%, PTH: 63.3±4.0%, SclAB: 68.0±5.6%, Fig 1I) than the VEH- and BIS-groups (VEH: 41.2±6.3%, BIS: 42.4%±3.3, Fig 1I). Bone resorption rate (BRR) was significantly reduced in all treatment groups (BIS: 0.6±0.2%/d; ML: 0.7±0.2%/d; PTH: 0.5±0.2%/d; SclAB: 0.5±0.2%/d; Fig 1J) compared to the VEH-group (VEH: 1.4±0.3%/d). Mineral resorption rate (MRR) was significantly reduced in the BIS-group (BIS: 1.1±0.1µm/d) compared to the VEH-group (1.7±0.2µm/d), being unchanged in the anabolic treatment groups (ML: 1.7±0.3µm/d; PTH: 1.6±0.1µm/d; SclAB: 1.7±0.2µm/d; Fig 1K). Eroded surface (ES) was significantly reduced in the anabolic treatment groups (ML: 22.0±4.6%; PTH: 19.5±3.2%; SclAB: 14.0±3.3%; Fig 1L), compared to the VEH- or the BIS-group (VEH: 30.6±4.9%; BIS: 29.5±3.9%;).

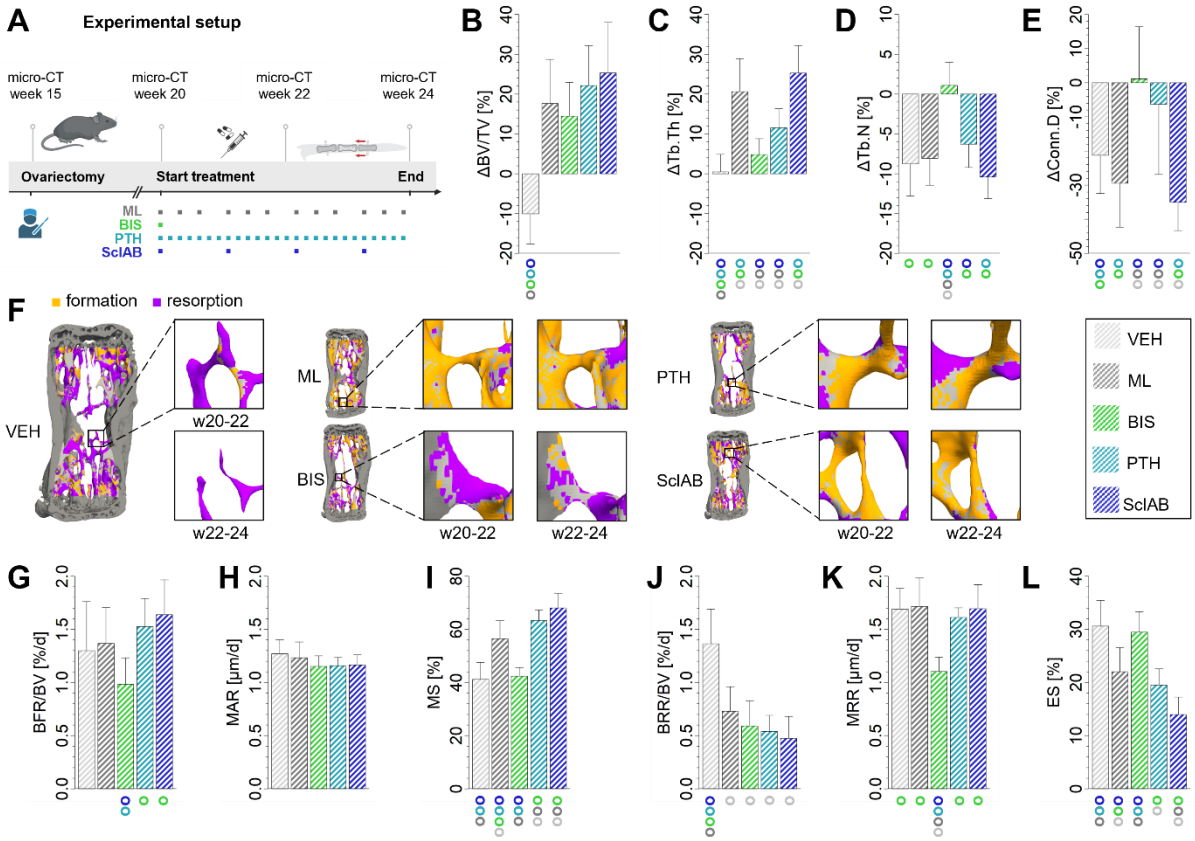

Figure 1: Monotreatments increase trabecular bone volume and architecture by different (re)modeling mechanisms. *(**A**) Experimental setup. 15-week-old mice are ovariectomized and treatment is administered between week 20 (w20) and 24 (w24). Created with Biorender (**B-E**) Monotreatments (VEH: n=29, BIS: n=9, PTH: n=10, SclAB: n=9), bar plots show percentage change over four weeks in (**B**) bone volume fraction ΔBV/TV, (**C**) trabecular thickness ΔTb.Th, (**D**) trabecular number ΔTb.N (**E**) connectivity density ΔConn.D (**F**) representative micro-computed tomography overlays at intervals w20-w22 and w22-w24, with (re)modeling volumes (**G-L**) (Re)modeling rates calculated from time interval w22-w24 (**G**) bone formation rate BFR (**H**) mineral apposition rate MAR (**I**) mineralizing surface MS (**J**) bone resorption rate BRR (**K**) mineral resorption rate MRR (**L**) eroded surface ES. The symbol '**o**' denotes p<0.05 using ANOVA with Tukey post-hoc test (to VEH: light grey; to ML: dark grey; to BIS: green; to PTH: cyan; to SclAB: blue).*

Morphometric effects in combination groups show synergisms in anabolic treatments

Next, we investigated to which extent mechanical loading could further increase the morphometric effects of the pharmaceutical treatment response. Trabecular microstructures and representative inlets of the combination groups are depicted in Fig 2A. The BIS + ML-group resulted in 28.0±4.4% increase in BV/TV (BIS: 14.4±8.5%; ML: 17.7±11.0%; Fig 2B, Table 1) which did not exceed the sum of the single treatment responses and was not statistically significant from the BIS-group. The anabolic treatment groups showed increases in BV/TV which exceeded the sum of the monotreatment responses (PTH: 22.1±10.0%; SclAB: 25.3±12.7%, PTH + ML: 46.3±16.8%, SclAB + ML: 59.4±21.1%), indicating synergistic behaviour. ΔTb.Th in the BIS + ML group was significantly higher than in the BIS group (Fig 2C), to an extent comparable to the ML-group. Tb.Th in the PTH + ML-group was significantly higher than in the PTH-group after four weeks, and was considered additive while in the SclAB + ML-group, the effect was considered synergistic. ΔTb.N was preserved in the BIS + ML group, even with additional mechanical loading (Fig 2D). Interestingly, ML as a monotreatment had reduced Tb.N, and this effect was blunted by additional BIS treatment. The loss of Tb.N observed in SclAB could not be reverted in SclAB + ML. Conn.D as a measure of the structural integrity and interconnectedness of the trabecular network, was preserved the most in BIS + ML, and PTH + ML (Fig 2E). Cortical BV/TV and cortical thickness (Ct.Th) showed synergistic behaviour in both anabolic treatment groups PTH + ML and SclAB + ML (Fig 2F,G).

BFR in the anabolic combination groups exceeded the sum of the monotreatment responses (Fig 2H). MAR in interval 20-22 was lowered in the SclAB-group and increased in the SclAB + ML-group (Fig 2I). MS in BIS + ML showed beneficial increases, in PTH + ML and SclAB + ML additive increases (Fig 2J). BRR was significantly reduced in all combination groups (Fig 2K), but in the BIS + ML-group, the observed reduction in BRR by BIS treatment was not altered by mechanical loading. The anabolic treatment groups showed additive reductions in BRR (Fig 2L). The BIS + ML group was characterized by decreases in MRR, which were not altered by mechanical loading. MRR was synergistically reduced in the PTH + ML group and additively reduced in the SclAB + ML-group. Synergistic decreases in ES were observed for PTH + ML and SclAB + ML (Fig 2M).

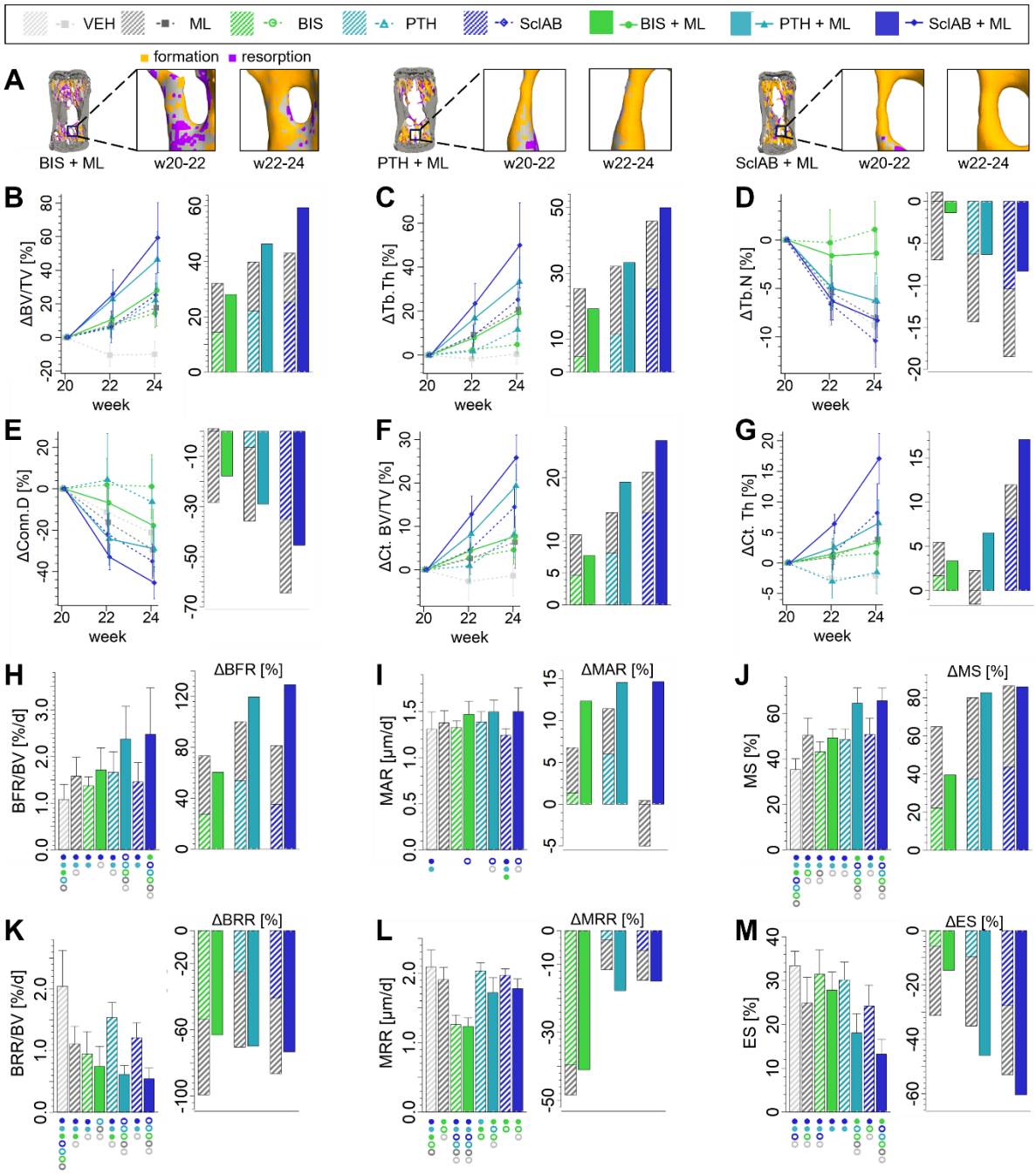

Figure 2: Mechanical loading increases the morphometric effects of anabolic but not anti-catabolic pharmaceutical treatments. *(**A**) Visual representations of combination groups BIS + ML, PTH + ML, and SclAB + ML in time intervals week (w) 20-22 and 22-24 (**B-M**) Change in parameter in % compared to week 20; sum of single vs. combined treatment indicating beneficial, additive or synergistic effects (**B**) bone volume fraction (ΔBV/TV) (**C**) trabecular thickness (ΔTb.Th) (**D**) trabecular number (ΔTb.N) (**E**) connectivity density (ΔConn.D) (**F**) cortical bone volume fraction (ΔCt.BV/TV) (**G**) cortical thickness (Ct.Th) (**H-M**) Dynamic bone morphometry calculated at biweekly time intervals week 20-22. Δ denotes change from VEH as no baseline value for dynamic bone morphometry rates was available. (**H**) bone formation rate per bone volume (BFR/BV) (**I**) mineral apposition rate (MAR) (**J**) mineralizing surface (MS) (**K**) bone resorption rate per bone volume (BRR/BV) (**L**) mineral resorption rate (MRR) (**M**) eroded surface (ES). Significances were calculated using ANOVA with Tukey post-hoc test; significant differences are depicted with a symbol in the color of the corresponding group (**o**: to monotreatment, ●: to combined treatment, $p<0.05$).*

Table 1: Significance levels of static morphometric parameters as difference from end of treatment at week 24 to start of treatment at week 20. *Significances were calculated using ANOVA with Tukey post-hoc test; significant differences are depicted with a symbol in the color of the corresponding group (**o**: to monotreatment, ●: to combined treatment, p<0.05).*

Parameter	VEH	ML	BIS	BIS + ML	PTH	PTH + ML	SclAB	SclAB + ML
ΔBV/TV [%]	ooo o●●●	o ●●	o ●●	o ●●	o ●●	ooooo ●	o ●●	ooooo ●
ΔTb.Th [%]	ooo ●●●	ooo ●●	oo ●●●	ooo ●●	ooo ●●●	ooooo ●●	ooo ●●	ooooo ●●
ΔTb.N [%]	o ●	o ●	oooo ●●	oooo ●●	o ●	o ●	o ●	o ●
ΔConn.D [%]	ooo ●	oo ●	ooo ●●●	oo ●●	ooo ●●	oo ●	oooo ●	oooo ●
ΔCt.BV/TV [%]	ooo o●●●	oo ●●	oo ●●	o ●●	oo ●●	oooo ●●	oooo ●	ooooo ●●
ΔCt.Th [%]	ooo ●●●	oo ●	ooo ●●	oo ●	ooo ●●●	ooo ●	ooo ●	ooooo ●●
ΔCt.BS/TV [%]	oo ●●	o ●●	oo ●	ooo ●	oooo ●●●	ooooo ●●	o ●	o ●

Mechanical properties as an indicator of fracture risk improve in all treatments

Decreased strength has been correlated to increased fracture risk. To investigate if increases in trabecular BV/TV were associated with increased trabecular strength thus giving indication of decreased fracture risk, we assessed mechanical properties of resulting structures over the course of four weeks. Trabecular strength increased in all treatment groups, with loading-induced increases being additive in the PTH + ML group and synergistic in the SclAB + ML group (Fig 3B). Mean strain energy density (SED) and maximum SED decreased in all treatment groups, being most pronounced in the combination groups with decreases being beneficial but less than additive (Fig 3C-D, Table 2). Linear regression analysis showed that the changes in trabecular strength and in BV/TV and Tb.Th correlated highly (BV/TV: w20-22: $R^2 = 0.84$, w22-24: $R^2 = 0.69$, Fig 3E; Tb.Th: w20-22: $R^2 = 0.78$, w22-24: $R^2 = 0.65$, Fig 3F).

To assess whether changes in strength arose rather from mineralizing and eroded surfaces or from changes in mineral apposition and resorption rates, the changes in strength were correlated with dynamic bone morphometric parameters. BFR and BRR correlated with increases in strength (BFR: w20-22: $R^2 = 0.77$, w22-24: $R^2 = 0.58$, Fig 3G,J). MS (w20-22: $R^2 = 0.75$, w22-24: $R^2 = 0.70$) and ES (w20-22: $R^2 = 0.71$, w22-24: $R^2 = 0.69$) correlated with increases in strength (Fig 3H,K). Low or no correlation was found for MAR (w20-22: $R^2 = 0.25$, w22-24: n.s.) and MRR (w20-22: $R^2 = 0.1$, w22-24: n.s.). These results indicate that increased bone volume, resulting primarily from a change in mineralizing and eroded surfaces, leads to increased trabecular strength. The higher linear regression coefficients in the first time interval than in the second time interval also suggest a time dependency of the treatment effects.

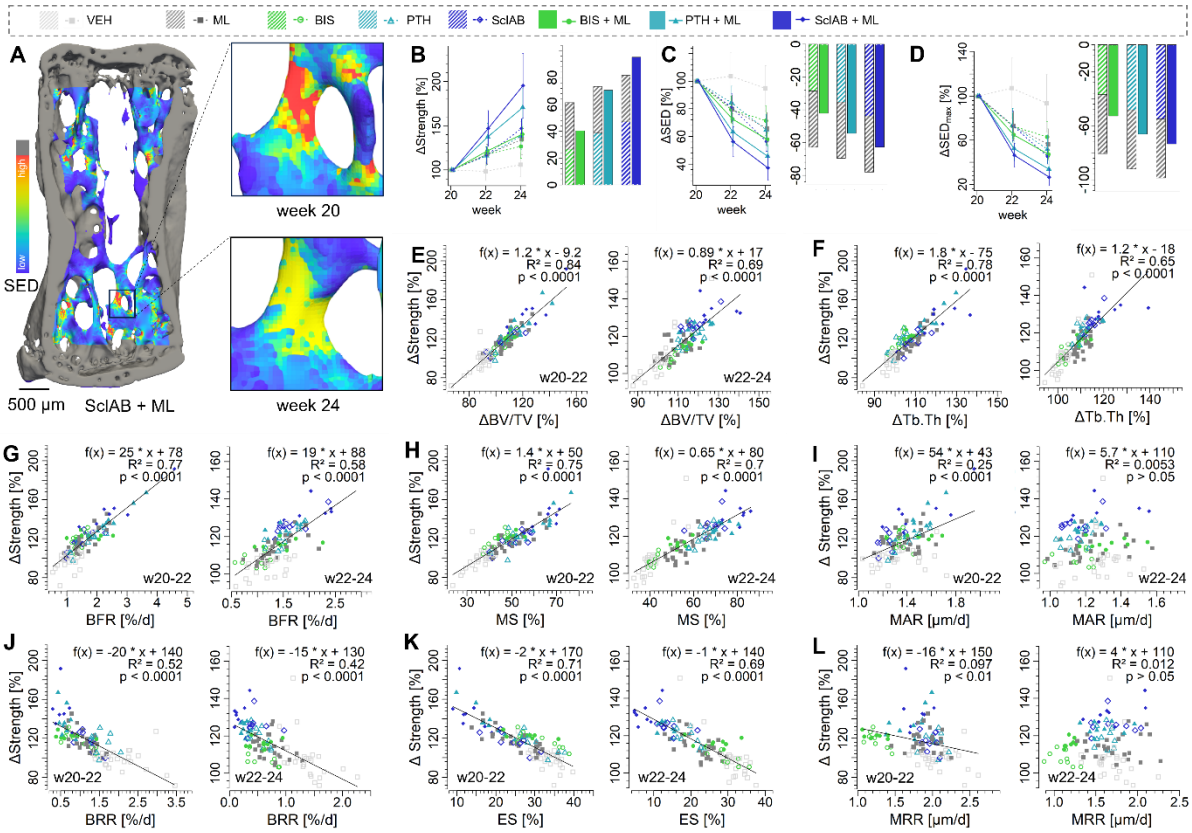

Figure 3: Trabecular strength increases by changes in mineralizing and eroded surfaces. *(**A**) Representative image of the strain-energy density (SED) distribution in the 6th caudal vertebra of a SclAB + ML animal and a zoom-in on a trabecular detail at week 20 and week 24, showing a heterogeneous site of high SED (week 20) and a structural reorganization resulting in a reduction in SED (week 24). (**B-D**) Change in mechanical properties over 4 weeks and sum of single treatment responses in parameter compared to combined treatment response. (**B**) ΔStrength (**C**) ΔSED (**D**) ΔSED maximum. (**E-L**) Linear regression analysis in biweekly intervals of ΔStrength and morphometric parameters in week intervals 20-22 and 22-24, (**E**) ΔBV/TV (**F**) ΔTb.Th (**G**) BFR (**H**) MS (**I**) MAR (**J**) BRR (**K**) ES (**L**) MRR.*

Table 2: Significance levels of mechanical properties*. Significances were calculated using ANOVA with Tukey post-hoc test; significant differences are depicted with a symbol in the color of the corresponding group (**o**: to monotreatment, ●: to combined treatment, p<0.05).*

Parameter	VEH	ML	BIS	BIS + ML	PTH	PTH + ML	SclAB	SclAB + ML
ΔSED [%]	OO ●●●	O ●	●●	O ●	●●	OOOO	O ●	OOOOO ●
ΔmaxSED [%]	OOO O●●●	O ●●	O ●●	O ●●	O ●●	OOOOO ●	O ●●	OOOOO ●
Δeff [%]	OOO O●●●	O ●●	O ●●	O ●	O ●●	OOOOO	O ●●	OOOOO ●
ΔStrength [%]	OOO O●●●	O ●●	O ●●	O ●	O ●	OOO ●	O ●	OOOOO ●●

Mechanical signal is higher in regions of bone formation than in regions of bone resorption.

To address the question whether pharmaceutical treatments target bone (re)modeling to the places that mechanically need it, we correlated the underlying mechanical signals in the trabecular compartment with subsequent formation and resorption events. Mean SED in resorption, quiescent, or formation volumes was calculated and normalized group-wise by mean quiescent SED to obtain relative mean SED-differences between (re)modeling events. Representative samples of each treatment group are illustrated in Fig 4. Visually, spatial agreement between sites of high SED and regions of subsequent bone formation, intermediate

strains and sites of quiescence, and low strains and sites of subsequent bone resorption can be found.

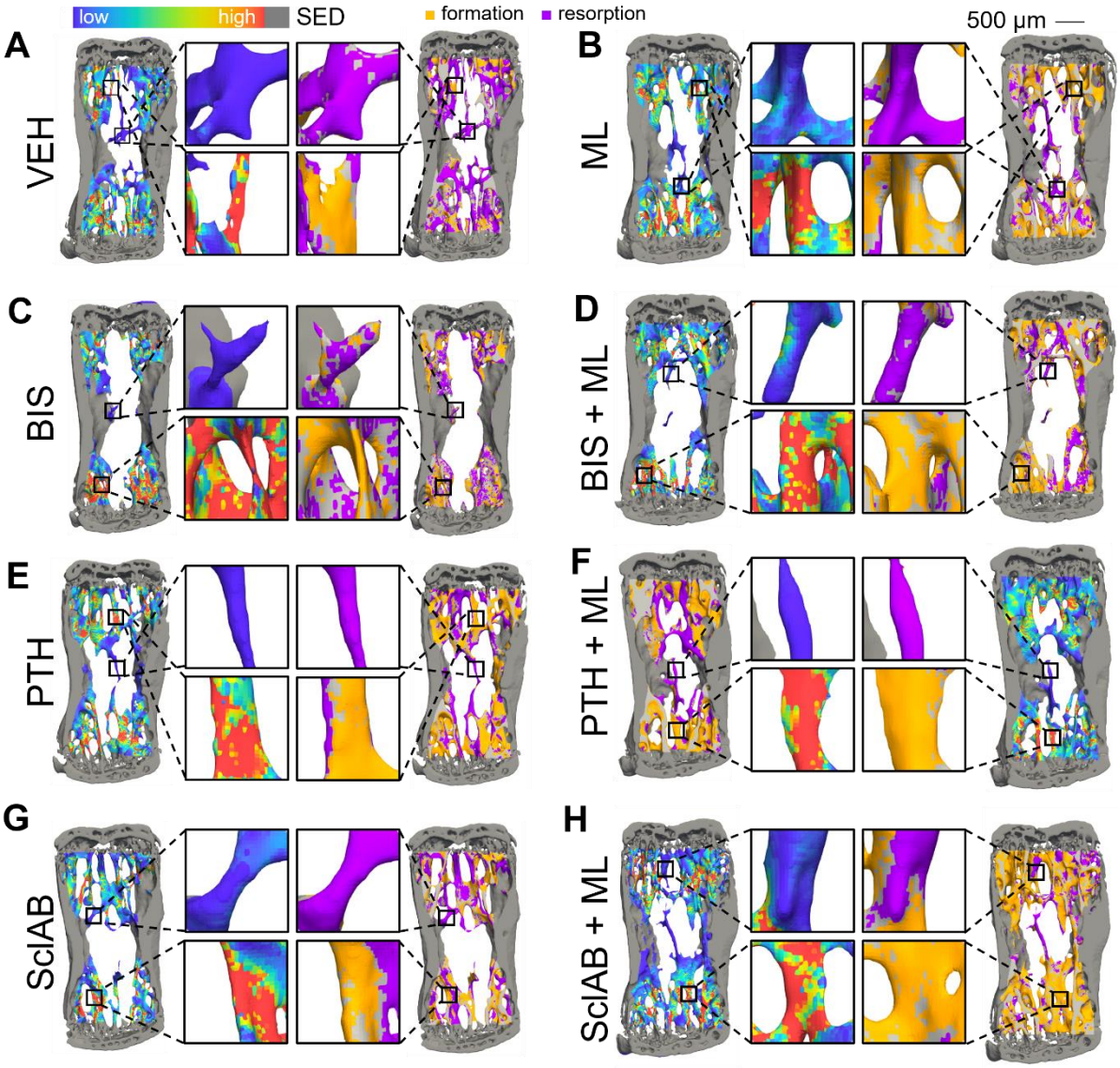

Figure 4: Formation occurs at high mechanical signal and resorption at low mechanical signal*: Three-dimensional mechanical environment (SED computed with micro-finite element analysis in the basal scan at week 20) compared to trabecular bone formation and resorption volumes over 2 weeks (week 22). The inlets show a magnified view of resorption and formation locations in individual trabeculae. Visual comparison reveals that high SED (red) matches with sites of bone formation (yellow), while low SED (blue) is predominantly found at locations of bone resorption (violet). (**A**) Slice of representative animal of the vehicle (VEH) (**B**) mechanical loading (ML) (**C**) bisphosphonate (BIS) (**D**) combined BIS + ML (**E**) parathyroid hormone (PTH), (**F**) combined PTH + ML (**G**) sclerostin antibody (SclAB), and (**H**) combined SclAB + ML group.*

Fig 5 shows mean SED at formation, quiescent and resorption sites expressed as percent difference from the mean (over all animals) quiescent SED, quantifying the observations of Fig 4. All groups showed significantly higher mean SED in formed volumes than in quiescent surfaces. Apart from the BIS and BIS + ML-groups, all groups demonstrated significantly lower SED-values in resorbed bone volumes than in quiescent surfaces. The addition of mechanical loading to the monotreatments resulted in marginal changes.

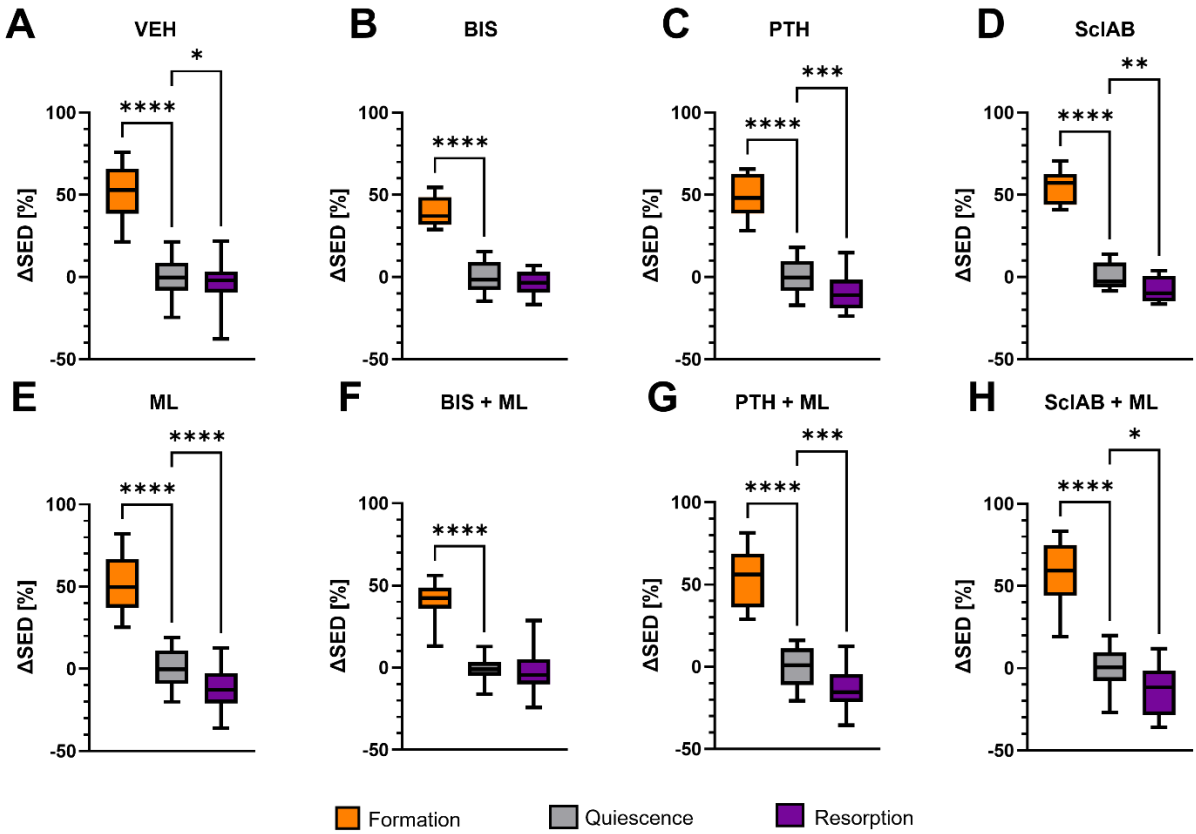

Figure 5: Mechanical signal is higher in regions of bone formation than in regions of bone resorption. *Relative differences of mean SED between quiescence, formation and resorption. SED values from the trabecular compartment were collected for all three (re)modeling events and compared to the mean SED value derived from quiescent surfaces.* ***(A)*** *Vehicle (VEH) group,* ***(B)*** *bisphosphonate (BIS) group,* ***(C)*** *parathyroid hormone (PTH) group* ***(D)*** *sclerostin antibody (SclAB) group),* ***(E)*** *mechanical loading (ML) group,* ***(F)*** *bisphosphonate and mechanical loading (BIS + ML) group,* ***(G)*** *PTH and mechanical loading (PTH + ML) group* ***(H)*** *SclAB and mechanical loading (SclAB + ML) group. Paired students t-test with Bonferroni correction; * $p<0.05$, ** $p<0.01$, *** $p<0.001$, **** $p<0.0001$.*

Mechanoregulation analysis shows differences between treatments

Next, we calculated the conditional probability curves of (re)modeling events (formation, quiescence, resorption) for a given SED-value. These curves were fitted with exponential functions. The probability for bone formation increased with increasing SED, and the probability for bone resorption decreased with increasing SED (Fig 6A-D). Mechanoregulation was more pronounced in ML compared to VEH (Fig 6A). BIS and BIS + ML showed lower slopes in the conditional probability curves than VEH (Fig 6B). PTH + ML showed higher slopes in the conditional probability curves compared to PTH (Fig 6C). In SclAB and SclAB + ML, the formation and resorption curves were shifted up and down respectively, while the slopes were not affected, meaning mechanical loading mainly affected non-targeted formation and resorption (Fig 6D).

Fig 6E-H shows parameters of interest extracted from the conditional probability curves (explained in Fig 6I). In ML, compared to VEH, non-targeted formation (VEH: 0.247, ML: 0.237; Fig 6E) and resorption (VEH: 0.245, ML: 0.21; Fig 6F) were decreased. BIS monotreatment increased non-targeted formation (0.258) compared to VEH (Fig 6 E,G) and resulted in the highest fraction of non-targeted resorption (0.258). Non-targeted formation in bisphosphonate-treated and loaded animals was the highest amongst all groups (BIS + ML: 0.268). While PTH alone decreased non-targeted formation (0.242), the effects were less than from ML (0.237), and the effects on non-targeted resorption (0.211) were similar to ML. The

PTH + ML group showed the lowest fraction of non-targeted formation (0.224) and resorption (0.181) among the investigated therapies. SclAB monotreatment decreased non-targeted formation (0.232) more than ML or PTH (Fig 6E). It decreased non-targeted resorption (0.235), but less than ML or PTH. Adding mechanical loading to SclAB increased non-targeted formation (0.238) to an extent where it was higher than ML but lower than PTH and resulted in lower non-targeted resorption (0.218) compared to SclAB.

BIS + ML had the lowest resorption/quiescent intersection value (Fig 6G), meaning there was only a small range where resorption probability was higher than quiescence and formation. PTH + ML had the highest intersection value, where resorption was most likely to occur for the biggest SED range. Only BIS and BIS + ML decreased this value compared to VEH. Only minor changes in the intersection between the quiescence and formation conditional probability curves were observed (Fig 6H). SclAB + ML was the only treatment that decreased this value compared to VEH, meaning formation probability was dominant over the largest SED range among all treatments.

The correct classification rate (CCR) summarizes the accuracy of the categorization into (re)modeling events: formation, resorption, quiescence, where a value of 0.33 would mean random mechanoregulation. CCR values of PTH + ML (0.505) and SclAB + ML (0.504) were significantly higher than VEH (0.471), demonstrating that to increase overall mechanoregulation, a combination of pharmaceutical treatment and mechanical loading was necessary (Fig 6J). BIS and BIS + ML showed significantly lower CCR values (0.447/0.448) than ML (0.491), PTH + ML, SclAB (0.487) and SclAB + ML. While SclAB monotreatment showed higher CCR values compared to BIS and BIS + ML, PTH (0.478) monotreatment did not significantly affect CCR values.

Area under the curve for the receiver operating characteristic for formation (AUC_F) and resorption (AUC_R) are descriptors for (re)modeling-specific mechanoregulation. Combined anabolic treatments resulted in increased mechanoregulation of bone formation with AUC_F values of 0.697 and 0.711 compared to VEH (0.615), ML (0.631), BIS (0.573) and BIS + ML (0.585). Only SclAB + ML showed a significant increase over PTH monotreatment (0.642). BIS and BIS + ML resulted in the lowest AUC_F across all groups. Mechanoregulation of bone resorption, reflected in AUC_R, was increased in ML (0.525), SclAB (0.531), BIS + ML (0.529), PTH + ML (0.555) and SclAB + ML (0.558) compared to VEH (0.513) (Fig 6L). Combined anabolic treatments had the greatest effect on AUC_R, with values being significantly higher than the other therapies. BIS (0.517) and PTH (0.526) monotreatment had no significant effect on AUC_R compared to VEH.

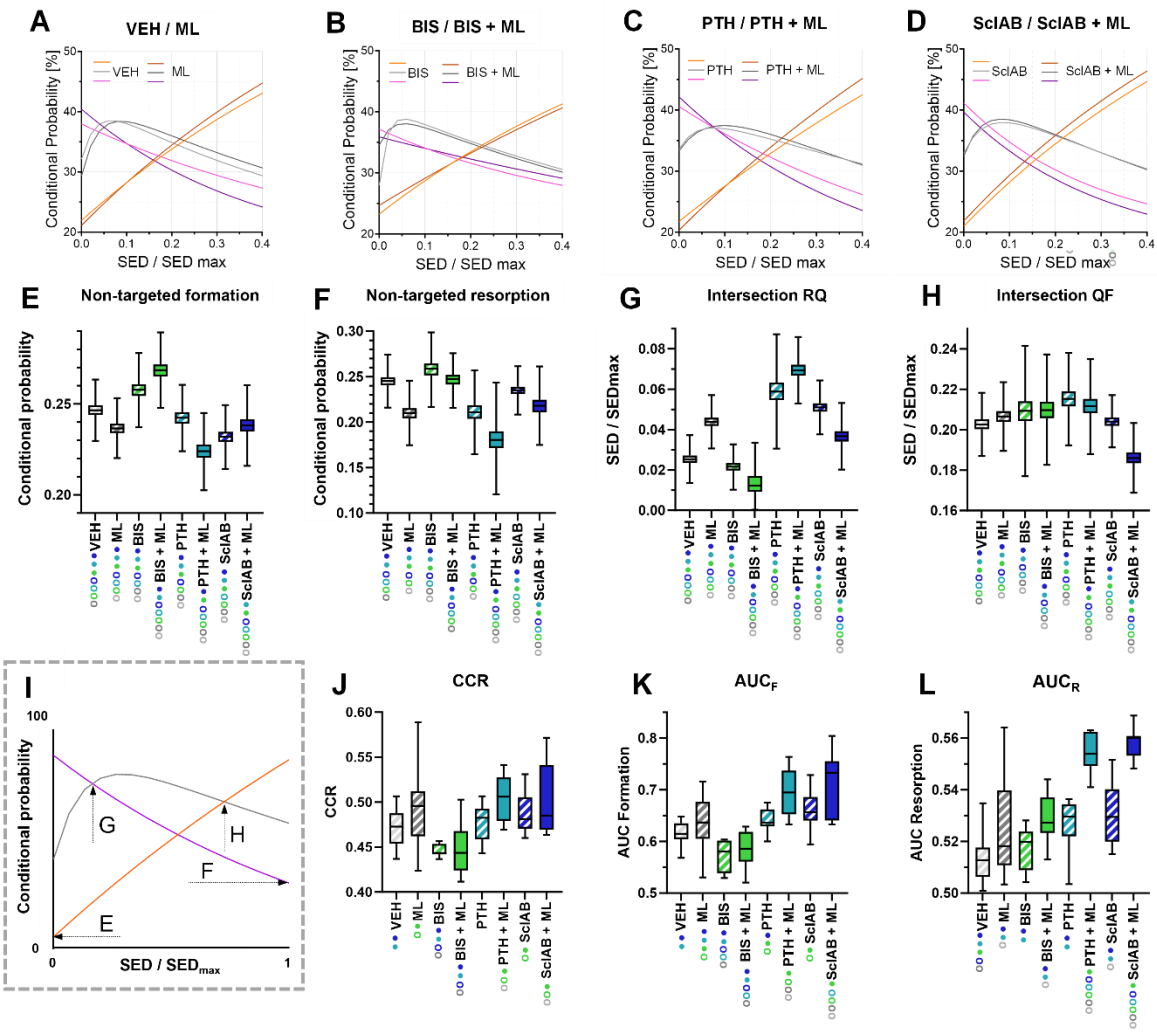

*Figure 6: Conditional probabilities and quantification of mechanoregulation show differences between treatments. **(A-D)** conditional probability curves, **(E-H)** points of interest from conditional probability curves, which are explained in **(I)** an example conditional probability curve, **(J)** CCR, **(K)** AUC formation, **(L)** AUC resorption. Significances were calculated with one-way Anova or Kruskal-Wallis based on normality with Tukey post-hoc-test and significant differences are depicted with a symbol in the color of the corresponding group (**o**: to monotreatment, ●: to combined treatment, $p<0.05$).*

Treatments effects on (re)modeling velocity curves and mechanostat parameters

To analyze how the investigated treatments influence the sensitivity of mechanoregulation mechanisms, we calculated mean (re)modeling velocity (RmV) curves (*18*) for each treatment group. These curves show the net RmV for a given surface effective strain, where a negative value means net resorption and a positive value means net formation. Minimum and maximum RmV, as well as (re)modeling thresholds (RTs) were extracted from the resulting curve. The RmV increased with increasing effective strain in all groups. Treatment increased RmV (Fig 7A-D), minimum and maximum RmV (Fig 7I,J), as well as decreased the RT for all groups but PTH + ML (Fig 7K) compared to VEH. PTH + ML did not have an RT as it increased the RmV especially for low strains, leading to net bone formation across the whole range of effective strains. Combined treatments generally led to increased RmVs compared to monotreatments, except for BIS + ML. Using VEH as the control, the RmV curve from ML was shifted up along the y-axis with a slight decrease in curvature (Fig 7A). BIS caused a RmV curve with a steep increase at low effective strain, after which the curve abruptly bent into an almost linear function with a low gradient. This effect was even more pronounced in BIS + ML. PTH increased RmV overall and decreased the curvature of the function compared to VEH/ML. PTH

+ ML led to an almost linear curve, except for a small increase for low effective strain. SclAB and SclAB + ML led to RmV curves that were most similar to VEH and ML and were only shifted up along the y-axis. The analysis of the minimum RmV (Fig 7I) showed that BIS + ML decreased it (-0.00585 µm/d) as compared to the respective monotreatments (BIS: -0.00169 µm/d; ML: -0.00343 µm/d), while it was increased by the other combined treatments as compared to their respective monotreatments. VEH (-0.00837 µm/d) resulted in the lowest and PTH + ML (0.00301 µm/d) in the highest minimum RmV. The maximum RmV (Fig 7J) was highest for SclAB + ML (0.00721 µm/d), even when compared to PTH + ML (0.00676 µm/d). BIS + ML (25.0 µε) resulted in the lowest RT, followed by SclAB + ML (35.0 µε) and BIS (70.0 µε) (not counting PTH + ML), while VEH resulted in the highest RT (1050.0 µε) (Fig 7K).

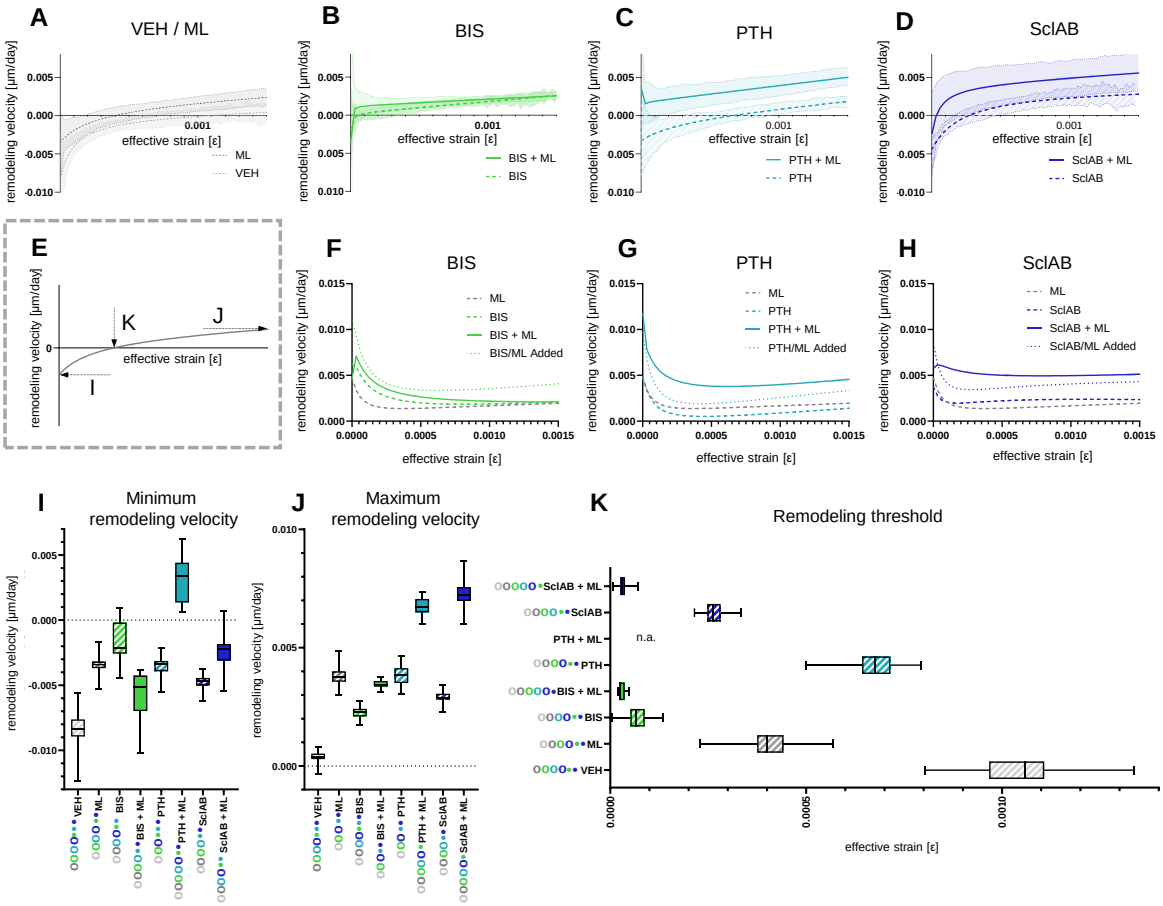

Figure 7: (Re)modeling velocity curves are altered by mono- and combined treatments. (A-D) *(re)modeling velocity (RmV) curves for* ***(A)*** *VEH / ML,* ***(B)*** *BIS / BIS + ML,* ***(C)*** *PTH / PTH + ML,* ***(D)*** *SclAB / SclAB + ML;* ***(E)*** *example RmV curve explaining the extracted parameters in I,J and K:* ***(I)*** *minimum RmV,* ***(J)*** *maximum RmV and* ***(K)*** *(re)modeling threshold (RT) of the mechanostat curves;* ***(F-H)****: treatment effects on the RmV curves comparing the effects of combined treatments with the respective monotreatments they consist of for* ***(F)*** *BIS / BIS + ML,* ***(G)*** *PTH / PTH + ML,* ***(H)*** *SclAB / SclAB + ML. Significances were calculated with Kruskal-Wallis test and Tukey post-hoc test; significant differences are depicted with a symbol in the color of the corresponding group (****o****: to monotreatment, ●: to combined treatment, p<0.05).*

To analyze the effects of combined treatments compared to monotreatments, we calculated the differences between each treatment-induced RmV curve and the VEH RmV curve. In order to gain a better insight into how effective a combination of treatments might be, we provided an overview of the treatment effects of the respective monotreatments, the effect of the combined treatment, and the theoretical effect of adding both monotreatment effects in Fig 7F-H. BIS + ML showed a larger effect on RmV than ML or BIS except for very high and very low strains. However, this effect was consistently lower than the addition of monotreatments and could thus

not be considered additive. Fig 7G shows that while PTH monotreatment increased RmV to a lesser extent than ML, the combined treatment was consistently higher than both monotreatment effects, indicating synergy. As demonstrated in Fig 7G, the effect of PTH + ML treatment was greatest for very low effective strain. SclAB monotreatments effects were higher than those of ML, and SclAB + ML combined caused a greater effect than the addition of the effects of the monotreatments, indicating synergism, except for <0.0001 effective strain (Fig 7H). In contrast to PTH + ML, SclAB + ML caused a more consistent increase across all effective strain levels, as suspected by the similar shape of the SclAB + ML RmV curve compared to VEH.

Fig 8A shows how the SED-distribution in trabecular bone changed over time in the three combined treatments and the control VEH. In the VEH group, in several areas, high SED values decreased over time, but in other areas they increased. Additionally, Fig 8A illustrates how the resorption of a single trabecula leads to a more heterogeneous SED distribution. While SED on average decreased over time for BIS + ML, this did not particularly affect areas with high SED, as there remained several highly strained areas in week 24. In contrast, both PTH + ML and SclAB + ML showed large decreases in SED, especially in areas with high SED values in week 20.

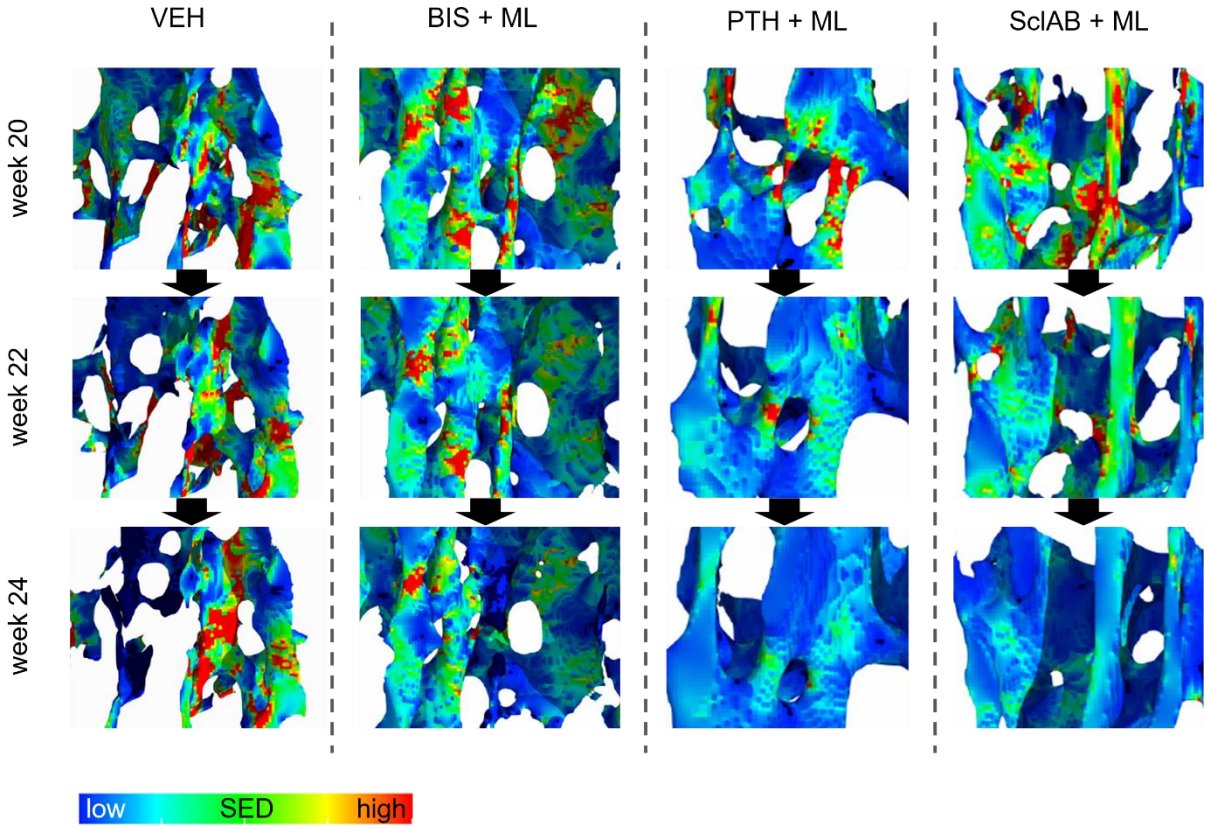

Figure 8: Mechanoregulation decreases the heterogeneity of the strain distribution to different extents in different treatments. *Qualitative comparison of changing SED-distribution for VEH, BIS + ML, PTH + ML and SclAB + ML over the course of 4 weeks of treatment.*

DISCUSSION

In this study, the effects of combining supraphysiological mechanical loading with anabolic and anti-catabolic pharmaceutical treatments in a mouse model of osteoporosis were investigated. Our findings suggest that combining physical with anabolic but not anti-catabolic osteoporosis treatments leads to a synergistic trabecular bone response and local

mechanoregulation compared to the respective monotreatments. Although bisphosphonate treatment was not impaired by combination with mechanical loading, the deleterious effects of bisphosphonates on mechanoregulation could not be recovered. PTH treatment benefitted most from mechanical loading, indicated by synergistically increased sensitivity of mechanoregulation mechanisms compared to monotreatment.

We found increased sensitivity of mechanoregulation mechanisms for PTH + ML but not for only PTH compared to VEH (Fig 6), which is in line with the results of Ryder et al (*26*), where PTH combined with fluid flow increased the mechanoresponse of osteoblasts, although PTH alone did not. Hagino et al. (*27*) hypothesized that PTH lowers the (re)modeling threshold of the (re)modeling velocity function, which our findings support (Fig 7). Notably, combining PTH with mechanical loading lowered the (re)modeling threshold to such an extent that the entire (re)modeling velocity curve was positive, meaning that even for very low effective strain, there is more formation than resorption, leading to net bone formation. These results are in agreement with data from studies by Miller et al. (*28*), where the effects of PTH + ML resulted in an overall increase of cortical thickness at zero longitudinal strain, and effects varied for different surface strains, suggesting altered mechanoregulation.

In the current study, sclerostin antibody treatment resulted in a synergistic increase in bone volume and strength when combined with mechanical loading. Bone formation rates were increased, and bone resorption rates were decreased as compared to single treatments, being in line with previous publications (*8, 29, 30*). SclAB and SclAB + ML groups both led to equally high degrees of mechanoregulation, showing similar curve characteristics for conditional probabilities of (re)modeling in relation to the mechanical environment and similar (re)modeling velocities. It has been suggested that the decoupling of bone formation and resorption caused by sclerostin antibodies is similar to the effect of mechanical loading, to the extent of being interchangeable (*31*). This might be relevant for patient groups that might not be suited for certain pharmaceutical treatment regimens, such as patients suffering from rheumatoid arthritis (*32*). While mechanical loading also uses sclerostin-independent pathways (*33*), our static, dynamic, mechanical, and mechanoregulation analysis suggested that sclerostin antibody treatment affects bone (re)modeling in a similar way. However, Morse et al. reported sclerostin antibody treatment combined with mechanical loading affected different genes related to the Wnt/β-catenin pathway (*23*), which could be a reason for a synergistic response elicited by the combination on the (re)modeling velocity curve. Occurring synergisms might be explained by the interplay between factors other than sclerostin in the mechanical response to loading. One candidate could be the Dickkopf-1 (Dkk1) protein which when inhibited in combination with sclerostin, resulted in a robust osteoanabolic effect in mice (*34*).

Bisphosphonates were the only treatment that preserved Tb.N compared to all other groups. Clinical studies on postmenopausal women found no effects of combination treatment (*35*), with differences of bisphosphonate treatment alone depending on the bone and site (*36*), while Kistler-Fischbacher et al. (*37*) found positive effects of bisphosphonate and mechanical loading treatment in the load-bearing femoral neck which were less pronounced in the spine, and also dependent on the kind of exercise. Stadelmann et al. (*38*) found additive effects on cortical thickness for several areas, however, bisphosphonates seemed to impair mechanical loading in regions of high strains, which suggested altered mechanosensation. In trabecular bone, Sugiyama et al. (*20*) found no improvements of combining bisphosphonates and mechanical loading in trabecular mouse tibial bone. This corroborates our finding of decreased mechanoregulation under bisphosphonate treatment (Fig 6J), which could not be recovered by additional mechanical loading and showed that bisphosphonates decreased bone formation where it was mechanically most needed (Fig 7J). Since mineralizing and eroded surfaces were similar in the bisphosphonate group compared to the vehicle group, our results suggest that

bisphosphonates not only affect the activity of osteoclasts but also that of osteoblasts. Namely, the coupling process between osteoclasts and osteoblasts could be disturbed by osteoclast apoptosis (*39*). Additionally, bisphosphonates impair osteoblast activation (*40*), likely affecting spatial distribution, where cells are less guided by the mechanical signal.

Regions with high local strain are linked to higher occurrences of microscopic tissue damage (*41*), of which even small amounts can cause large reductions in strength (*42*) and increase fatigue fracture risk (*43*). While bone mass is a well-established indicator for assessing mechanical performance in bone research (*42*), our findings indicate that mechanoregulation also significantly contributes to our understanding of bone health and functionality. This means that not only the quantity of bone tissue but also the ability of the bone to utilize its regulatory mechanisms in response to mechanical stimuli plays a crucial role in maintaining and improving bone strength. Cosman et al. (*44*) reported a decrease in vertebral fractures after monthly sclerostin antibody treatment in postmenopausal women, where fatigue fractures are common (*45*), but not in other bones. This supports our conclusion, that increases in mechanoregulation induced by sclerostin antibody treatment can help decrease fatigue fracture risk.

A limitation of this study is the use of mice as a model for human skeletal metabolism. While our results suggest that mechanical loading is of importance for therapeutic success, clinical studies will be required to determine how and through which specific types of physical activity this can be translated to humans. Similar to finding a suitable dose regimen with pharmaceuticals, optimizing specific exercise protocols is essential given that treatment outcomes depend on the type of exercise performed. In future translational studies, exercise-based loading programs might represent a relevant clinical scenario how treatment regimens can be combined, and the potential of synergistic effects can be exploited. As was found in the FRAME clinical trial, bone-forming effects of Romosozumab, a clinical version of sclerostin antibodies, on periosteal surfaces may require mechanical loading and potentially only manifest themselves in weight-bearing sites (*46*). Twelve months resistance or jump training as well as running a marathon reportedly decreased sclerostin levels (*47, 48*).

In conclusion, the current study revealed that I) pharmaceutical treatments target trabecular bone (re)modeling to the places that mechanically needed it, II) the combination of anabolic osteoporosis treatments and mechanical loading increased the trabecular bone response synergistically, and III) anabolic treatments in combination with supraphysiological mechanical loading led to synergistically increased mechanoregulation. This suggests that load-bearing physical therapy could improve the outcomes of osteoporosis patients treated with anabolic therapies, with load-bearing physical activity ensuring that anabolic effects in trabecular bone are better targeted to the mechanical needs, and ultimately leading to decreased fracture risk. Load-bearing physical activity may represent an additional treatment option especially for osteoporosis patients on anabolic osteoporosis therapy who are still physically active.

MATERIALS AND METHODS

Study design

The study design is illustrated in Fig 1A. In total, 120 female 15-week-old C57BL/6 mice (n=60, C57BL/JRccHsd, RCC/Harlan; Füllinsdorf, Switzerland/ Horst, The Netherlands; n=60, C57BL/6JRj mice (Janvier Labs, Le Genest-Saint-Isle, France) were subjected to bilateral ovariectomy. A basal micro-CT image of the 6th caudal vertebra was obtained (Scanco Medical, Brüttisellen, Switzerland). Recovery lasted five weeks after surgery, as in this period, an osteopenic state was established in the trabecular compartment of the 6th caudal vertebra in

a previous study (*49*). Pinning of the adjacent vertebrae as preparation for the loading procedure took place in week 17. At week 20, the animals were divided into 8 groups and the following treatments were administered for the following four weeks: BIS (n=9), BIS + ML (n=9), PTH (n=10), PTH + ML (n=9), SclAB (n=9), SclAB + ML (n=8), ML (n=26), VEH (n=25). 10 mice were excluded due to swollen tails or loose pins. In the SclAB study, 4 mice showed a periosteal reaction, possibly due to injury of the periosteum during intravenous injection at the tail vein. One mouse in the BIS + ML group did not lose bone volume after ovariectomy. These mice were excluded from evaluation, resulting in 105 animals included. Micro-CT was performed in weeks 15, 20, 22 and 24. Surgeries, imaging, and loading were performed under isoflurane anesthesia (induction 4%, maintenance 1.5-2.5%, Attane, Piramal Healthcare, India). Vehicle control was an isotonic buffer (pH 5.3). While the data was gained in four experiments (at different times), study and loading parameters were not different except for the administered pharmaceutical treatments, thus combined in this study. The bone responses of the VEH and the ML groups of both mouse lines (JRccHsd and 6JRj) showed no differences in reactions ($\Delta BV/TV_{w20-24;}$ VEH: $p = 0.937$; ML: $p = 0.206$; two-way ANOVA with Tukey post-hoc test), thus ML groups from all experiments and VEH groups from all experiments were merged, explaining the larger sample size in these groups. All animal experiments were performed with approval of the local authority (Kantonales Veterinäramt Zürich, Zurich, Switzerland).

Mechanical loading

To induce a bone response under controlled loading conditions, we used an *in vivo* mouse tail loading model of trabecular bone adaptation (*49-51*). Three weeks before loading start, pins were inserted into the 5th and 7th caudal vertebra under fluoroscopic control. At loading start, the 6th caudal vertebra (CV6) was subjected to cyclic mechanical loading at a force of 8N (or 0N sham loading) delivered through a specifically designed CVAD loading device, 3 times/week for 4 weeks at 10 Hz and 3000 cycles.

Pharmaceutical treatment

The BIS group received 100 µg/kg zoledronate (Zometa 4 mg/5 ml; Novartis Pharma Schweiz AG, Bern) subcutaneously once in week 20. Corresponding VEH (0.9% NaCl, B. Braun Medical AG, Switzerland) was injected at the same time point. Mice in the PTH study received 40 µg/kg PTH (hPTH 1-34, Bachem AG, Switzerland) or the according VEH (0.9% NaCl) subcutaneously daily over four weeks. SclAB (100 mg/kg, Novartis Pharma AG, Basel, Switzerland) or the corresponding VEH (isotonic buffer, pH 5.3) was injected weekly over 4 weeks.

Bone morphometry

Micro-CT images were obtained with a vivaCT 40 (Scanco Medical AG, Brüttisellen, Switzerland) operated at 55 kVp and 146 µA. 1000 projection images were obtained with an integration time of 200 ms. Grayscale images were reconstructed using a Feldkamp algorithm, with automated beam hardening correction, resulting in an isotropic voxel size of 10.5 µm. The image of week 20 was aligned in the main loading direction. Follow up scans were registered to the previous scan. A constrained 3D Gauss filter (sigma 1.2, support 1) and a global thresholding procedure (580 mgHA/cm^3) were applied. Automated masks were created to extract the trabecular bone volumes (trabecular mask truncated by 10% of length at both ends to exclude epiphyses and primary spongiosa; middle 26% removed because this area is almost void of trabeculae) (*25*). Static trabecular bone morphometric parameters were calculated

according to Bouxsein et al. (*52*). Dynamic bone morphometry was performed by registering and superimposing segmented bone volume images of consecutive time points. Bone formation and resorption rates were calculated as described previously (*53*) over two two-week periods (20-22 and 22-24).

Finite element analysis of mechanical properties

Finite-element simulations were used to analyze mechanical properties of the vertebrae. 3D micro-FE models were generated by converting all voxels of the micro-CT image to 8 node hexahedral elements, with each model consisting of approximately 1.8 million elements. A Young's modulus of 14.8 GPa and a Poisson's ratio of 0.3 (*50*) were assigned. Each model was solved with ParOSol (*54*) running on the Euler cluster operated by Scientific IT Services at ETH Zurich. Cylindric intervertebral disks (10% of absolute height) were applied and assigned the same Young's modulus and Poisson's ratio as bone. The top of the model was displaced by 1% of the total vertebral length, while the bottom was fixed. The resulting reaction force was rescaled to the value of the force applied in the experimental setup; consequently, all the FE outcomes were rescaled accordingly (4 N for non-loaded (*55*) and 8 N for loaded mice). Strain energy density (SED), defined as the increase in energy associated with the tissue deformation per unit volume, and effective strain were used as the mechanical signal. Trabecular bone strength was estimated for each mouse at each time point by using the Pistoia criterion (*56*) which assumes that bone failure is initiated if a certain percentage of the bone tissue (2%) is strained beyond the tissue yield effective strain (7000 $\mu\varepsilon$). For the trabecular bone strength estimation, the full bone was modeled but only the effective strains in the trabecular compartment were analyzed.

Mechanoregulation analysis

To associate sites of formation or resorption with the local mechanical environment on the trabecular bone surface, the mechanical environment at week 20 was projected into the volumetric formation and resorption clusters from week 20 to 22 using the method published by Griesbach et al. (*19*). The two volumetric clusters for formation and resorption as well as the quiescent surface of the superimposed micro-CT scans were used as masks and applied to the SED image. Mean SED values from these clusters were calculated and normalized by mean quiescent SED of each group (*12*). Area under the curve for the receiver operating characteristic were calculated for formation (AUC_F) and resorption (AUC_R) based on the respective clustered mechanical values and the mechanical values on the bone surface (*19, 51*).

Conditional probabilities were calculated for each (re)modeling event by creating histograms of SED values with 50 bins for formed, quiescent and resorbed bone volumes, rescaling them to contain the same amount of values to remove dependencies on imbalances in the (re)modeling process due to differences between animals or treatments, and consequently dividing the rescaled histograms bin-wise by the sum of the three (re)modeling histograms (*12*).

Mean conditional probabilities were calculated for all animals within one group and fitted with exponential functions. To compare parameters extracted from these functions, a bootstrapping approach was used by creating 2500 subsamples from each group (*18, 57*), fitting the conditional probability functions to the mean curve of each subsample. For formation and resorption, the minimum probability, indicating the amount of non-targeted formation or resorption, was compared between groups. Additionally, the intersections between the resorption and quiescent curve, and the quiescent and formation curve were computed. Furthermore, CCR values were calculated from the mean conditional probabilities from all

animals, returning a scalar value between 0.33 and 1 assessing overall mechanoregulation, with 0.33 meaning (re)modeling is independent of the mechanical signal and 1 meaning it is entirely dependent on the mechanical signal.

(Re)modeling velocities (RmVs) and their mechanostat parameters were calculated according to Marques et al. for each animal (*18*). As treatments altered the curve characteristics (Fig 7), we extended the hyperbolic curve fit used by Marques et al. by adding a linear component $RmV(x) = y_0 - \frac{a}{b*x} + c * x$ and fitted it to the mean RmV curve for each group. Minimum and maximum RmV, as well as (re)modeling thresholds (RTs) were extracted from the resulting curve. To enable statistical comparison of parameters derived from the curve fits, we used a bootstrapping approach creating 2500 subsamples from each group and fitting the extended hyperbolic function to the mean RmV curve of each subsample (*18, 57*). To compare treatment effects, we subtracted each RmV curve with the control RmV curve for the VEH group. The result represented the respective treatment effect on the RmV over the relevant effective strain values for each group. Additionally, we added the treatment effect of each pharmaceutical treatment to the effect of the ML group, to use as a reference of comparison for the combined treatment and assess and visualize if the effect was additive or even synergistic (*28*).

Statistical methods

Morphometric parameters were normalized to treatment start (week 20) for each animal. For the effect of ovariectomy, statistical analysis was performed using one-way ANOVA. Static, dynamic, and mechanical treatment effects were compared using two-way ANOVA over time and group with Tukey post-hoc-test. Synergism was defined as when the combined treatment exceeded the sum of the two single treatments. Additivity was defined as when the combined treatment was equal to the sum of the two single treatments. Comparison of parameters of the mechanoregulation analysis was performed using Kruskal-Wallis-Test with Tukey post-hoc test. Correlations were assessed with Pearson's coefficient and R^2. Statistical analysis was performed using R (R, Auckland, New Zealand, (*58*)) and GraphPad Prism 10 (GraphPad software, Boston, United States). Data are presented as mean ± standard deviation unless otherwise specified. P-values lower than 0.05 are considered significant.

Acknowledgments

We acknowledge Kathleen Koch for assistance and performance of animal experiments of the PTH and BIS groups, and Dr. Ulrike Kettenberger for assistance and performance of animal experiments of the PTH group. Finite element simulations were performed on the Euler cluster operated by Scientific IT Services at ETH Zurich.

Funding

European Union grant, VPHOP FP7-ICT-2008-223865 (FS, FML, GK, CW)
European Research Council, ERC Advanced, MechAGE ERC-2016-ADG-741883 (FCM, GK)

Author contributions

Conceptualization: RM, GAK, PJR
Methodology: CW, GAK, MS, FML
Investigation: JG, FAS, CW, MS, FML, GAK, FCM

Visualization: FAS, JG
Funding acquisition: RM, GAK
Project administration: GAK, RM
Supervision: RM, GAK, PJR
Writing – original draft: FAS, JG
Writing – review & editing: CW, MS, FML, FCM, PJR, MK, GAK, RM

Competing interests

M.K. and P.R. are employees of Novartis. The other authors declare they have no competing interests.

Data and materials availability

All data are available in the main text.

References

1. J. A. Kanis, E. V. McCloskey, H. Johansson, A. Oden, L. J. Melton, N. Khaltaev, A reference standard for the description of osteoporosis. *Bone* **42**, 467-475 (2008).
2. F. Al Anouti, Z. Taha, S. Shamim, K. Khalaf, L. Al Kaabi, H. Alsafar, An insight into the paradigms of osteoporosis: From genetics to biomechanics. *Bone Rep* **11**, (2019).
3. B. Busse, H. A. Bale, E. A. Zimmermann, B. Panganiban, H. D. Barth, A. Carriero, E. Vettorazzi, J. Zustin, M. Hahn, J. W. Ager, 3rd, K. Puschel, M. Amling, R. O. Ritchie, Vitamin D deficiency induces early signs of aging in human bone, increasing the risk of fracture. *Sci Transl Med* **5**, 193ra188 (2013).
4. B. Abrahamsen, D. Brask-Lindemann, K. H. Rubin, P. Schwarz, A review of lifestyle, smoking and other modifiable risk factors for osteoporotic fractures. *Bonekey Rep* **3**, 574 (2014).
5. K. W. Lyles, C. S. Colón-Emeric, J. S. Magaziner, J. D. Adachi, C. F. Pieper, C. Mautalen, L. Hyldstrup, C. Recknor, L. Nordsletten, K. A. Moore, C. Lavecchia, J. Zhang, P. Mesenbrink, P. K. Hodgson, K. Abrams, J. J. Orloff, Z. Horowitz, E. F. Eriksen, S. Boonen, Zoledronic acid and clinical fractures and mortality after hip fracture. *New Engl J Med* **357**, 1799-1809 (2007).
6. R. M. Neer, C. D. Arnaud, J. R. Zanchetta, R. Prince, G. A. Gaich, J. Y. Reginster, A. B. Hodsman, E. F. Eriksen, S. Ish-Shalom, H. K. Genant, O. Wang, B. H. Mitlak, Effect of parathyroid hormone (1-34) on fractures and bone mineral density in postmenopausal women with osteoporosis. *N Engl J Med* **344**, 1434-1441 (2001).
7. R. Baron, M. Kneissel, WNT signaling in bone homeostasis and disease: from human mutations to treatments. *Nat Med* **19**, 179-192 (2013).
8. M. S. Ominsky, R. W. Boyce, X. Li, H. Z. Ke, Effects of sclerostin antibodies in animal models of osteoporosis. *Bone* **96**, 63-75 (2017).
9. K. G. Saag, J. Petersen, M. L. Brandi, A. C. Karaplis, M. Lorentzon, T. Thomas, J. Maddox, M. Fan, P. D. Meisner, A. Grauer, Romosozumab or Alendronate for Fracture Prevention in Women with Osteoporosis. *N Engl J Med* **377**, 1417-1427 (2017).
10. I. Hoffmann, M. Kohl, S. von Stengel, F. Jakob, K. Kerschan-Schindl, U. Lange, S. Peters, D. Schoene, C. Sieber, F. Thomasius, H. A. Bischoff-Ferrari, M. Uder, W. Kemmler, Exercise and the prevention of major osteoporotic fractures in adults: a systematic review and meta-analysis with special emphasis on intensity progression and study duration. *Osteoporos Int* **34**, 15-28 (2023).

11. H. M. Frost, Bone's mechanostat: a 2003 update. *Anat Rec A Discov Mol Cell Evol Biol* **275**, 1081-1101 (2003).
12. F. A. Schulte, D. Ruffoni, F. M. Lambers, D. Christen, D. J. Webster, G. Kuhn, R. Muller, Local mechanical stimuli regulate bone formation and resorption in mice at the tissue level. *PLoS One* **8**, e62172 (2013).
13. H. Razi, A. I. Birkhold, R. Weinkamer, G. N. Duda, B. M. Willie, S. Checa, Aging Leads to a Dysregulation in Mechanically Driven Bone Formation and Resorption. *J Bone Miner Res* **30**, 1864-1873 (2015).
14. P. Christen, K. Ito, R. Ellouz, S. Boutroy, E. Sornay-Rendu, R. D. Chapurlat, B. van Rietbergen, Bone remodelling in humans is load-driven but not lazy. *Nat Commun* **5**, 4855 (2014).
15. M. Walle, F. C. Marques, N. Ohs, M. Blauth, R. Muller, C. J. Collins, Bone Mechanoregulation Allows Subject-Specific Load Estimation Based on Time-Lapsed Micro-CT and HR-pQCT in Vivo. *Front Bioeng Biotechnol* **9**, 677985 (2021).
16. D. B. Burr, Targeted and nontargeted remodeling. *Bone* **30**, 2-4 (2002).
17. J. M. Graham, B. P. Ayati, S. A. Holstein, J. A. Martin, The role of osteocytes in targeted bone remodeling: a mathematical model. *PLoS One* **8**, e63884 (2013).
18. F. C. Marques, D. Boaretti, M. Walle, A. C. Scheuren, F. A. Schulte, R. Müller, Mechanostat parameters estimated from time-lapsed micro-computed tomography data of mechanically driven bone adaptation are logarithmically dependent on loading frequency. *Front Bioeng Biotech* **11**, (2023).
19. J. K. Griesbach, F. A. Schulte, G. N. Schadli, M. Rubert, R. Muller, Mechanoregulation analysis of bone formation in tissue engineered constructs requires a volumetric method using time-lapsed micro-computed tomography. *Acta Biomater*, (2024).
20. T. Sugiyama, L. B. Meakin, G. L. Galea, B. F. Jackson, L. E. Lanyon, F. H. Ebetino, R. G. Russell, J. S. Price, Risedronate does not reduce mechanical loading-related increases in cortical and trabecular bone mass in mice. *Bone* **49**, 133-139 (2011).
21. T. Sugiyama, L. K. Saxon, G. Zaman, A. Moustafa, A. Sunters, J. S. Price, L. E. Lanyon, Mechanical loading enhances the anabolic effects of intermittent parathyroid hormone (1-34) on trabecular and cortical bone in mice. *Bone* **43**, 238-248 (2008).
22. L. B. Meakin, H. Todd, P. J. Delisser, G. L. Galea, A. Moustafa, L. E. Lanyon, S. H. Windahl, J. S. Price, Parathyroid hormone's enhancement of bones' osteogenic response to loading is affected by ageing in a dose- and time-dependent manner. *Bone* **98**, 59-67 (2017).
23. A. Morse, A. Schindeler, M. M. McDonald, M. Kneissel, I. Kramer, D. G. Little, Sclerostin Antibody Augments the Anabolic Bone Formation Response in a Mouse Model of Mechanical Tibial Loading. *J Bone Miner Res* **33**, 486-498 (2018).
24. S. T. Robinson, P. T. Shyu, X. E. Guo, Mechanical loading and parathyroid hormone effects and synergism in bone vary by site and modeling/remodeling regime. *Bone* **153**, 116171 (2021).
25. F. M. Lambers, F. A. Schulte, G. Kuhn, D. J. Webster, R. Muller, Mouse tail vertebrae adapt to cyclic mechanical loading by increasing bone formation rate and decreasing bone resorption rate as shown by time-lapsed in vivo imaging of dynamic bone morphometry. *Bone* **49**, 1340-1350 (2011).
26. K. D. Ryder, R. L. Duncan, Parathyroid hormone modulates the response of osteoblast-like cells to mechanical stimulation. *Calcif Tissue Int* **67**, 241-246 (2000).
27. H. Hagino, T. Okano, M. P. Akhter, M. Enokida, R. Teshima, Effect of parathyroid hormone on cortical bone response to in vivo external loading of the rat tibia. *J Bone Miner Metab* **19**, 244-250 (2001).
28. C. J. Miller, S. Trichilo, E. Pickering, S. Martelli, E. Dall'Ara, P. Delisser, L. B. Meakin, P. Pivonka, Cortical thickness adaptation to combined mechanical loading and parathyroid hormone treatments is site specific and synergistic in the mouse tibia model. *Bone* **180**, 116994 (2024).
29. S. Taylor, M. S. Ominsky, R. Hu, E. Pacheco, Y. D. He, D. L. Brown, J. I. Aguirre, T. J. Wronski, S. Buntich, C. A. Afshari, I. Pyrah, P. Nioi, R. W. Boyce, Time-dependent cellular and transcriptional changes in the osteoblast lineage associated with sclerostin antibody treatment in ovariectomized rats. *Bone* **84**, 148-159 (2016).

30. M. S. Ominsky, S. K. Boyd, A. Varela, J. Jolette, M. Felx, N. Doyle, N. Mellal, S. Y. Smith, K. Locher, S. Buntich, I. Pyrah, R. W. Boyce, Romosozumab Improves Bone Mass and Strength While Maintaining Bone Quality in Ovariectomized Cynomolgus Monkeys. *Journal of Bone and Mineral Research* **32**, 788-801 (2017).
31. T. Sugiyama, T. Torio, T. Miyajima, Y. T. Kim, H. Oda, Romosozumab and blosozumab: alternative drugs of mechanical strain-related stimulus toward a cure for osteoporosis. *Front Endocrinol (Lausanne)* **6**, 54 (2015).
32. C. Wehmeyer, S. Frank, D. Beckmann, M. Bottcher, C. Cromme, U. Konig, M. Fennen, A. Held, P. Paruzel, C. Hartmann, A. Stratis, A. Korb-Pap, T. Kamradt, I. Kramer, W. van den Berg, M. Kneissel, T. Pap, B. Dankbar, Sclerostin inhibition promotes TNF-dependent inflammatory joint destruction. *Sci Transl Med* **8**, 330ra335 (2016).
33. A. Morse, M. M. McDonald, N. H. Kelly, K. M. Melville, A. Schindeler, I. Kramer, M. Kneissel, M. C. van der Meulen, D. G. Little, Mechanical load increases in bone formation via a sclerostin-independent pathway. *J Bone Miner Res* **29**, 2456-2467 (2014).
34. P. C. Witcher, S. E. Miner, D. J. Horan, W. A. Bullock, K. E. Lim, K. S. Kang, A. L. Adaniya, R. D. Ross, G. G. Loots, A. G. Robling, Sclerostin neutralization unleashes the osteoanabolic effects of Dkk1 inhibition. *JCI Insight* **3**, (2018).
35. K. Uusi-Rasi, P. Kannus, S. Cheng, H. Sievanen, M. Pasanen, A. Heinonen, A. Nenonen, J. Halleen, T. Fuerst, H. Genant, I. Vuori, Effect of alendronate and exercise on bone and physical performance of postmenopausal women: a randomized controlled trial. *Bone* **33**, 132-143 (2003).
36. P. D. Chilibeck, K. S. Davison, S. J. Whiting, Y. Suzuki, C. L. Janzen, P. Peloso, The effect of strength training combined with bisphosphonate (etidronate) therapy on bone mineral, lean tissue, and fat mass in postmenopausal women. *Can J Physiol Pharmacol* **80**, 941-950 (2002).
37. M. Kistler-Fischbacher, J. S. Yong, B. K. Weeks, B. R. Beck, A Comparison of Bone-Targeted Exercise With and Without Antiresorptive Bone Medication to Reduce Indices of Fracture Risk in Postmenopausal Women With Low Bone Mass: The MEDEX-OP Randomized Controlled Trial. *J Bone Miner Res* **36**, 1680-1693 (2021).
38. V. A. Stadelmann, N. Bonnet, D. P. Pioletti, Combined effects of zoledronate and mechanical stimulation on bone adaptation in an axially loaded mouse tibia. *Clin Biomech (Bristol, Avon)* **26**, 101-105 (2011).
39. N. A. Sims, T. J. Martin, Osteoclasts Provide Coupling Signals to Osteoblast Lineage Cells Through Multiple Mechanisms. *Annu Rev Physiol* **82**, 507-529 (2020).
40. P. R. Jensen, T. L. Andersen, P. Chavassieux, J. P. Roux, J. M. Delaisse, Bisphosphonates impair the onset of bone formation at remodeling sites. *Bone* **145**, (2021).
41. M. G. Goff, F. M. Lambers, R. M. Sorna, T. M. Keaveny, C. J. Hernandez, Finite element models predict the location of microdamage in cancellous bone following uniaxial loading. *J Biomech* **48**, 4142-4148 (2015).
42. C. J. Hernandez, F. M. Lambers, J. Widjaja, C. Chapa, C. M. Rimnac, Quantitative relationships between microdamage and cancellous bone strength and stiffness. *Bone* **66**, 205-213 (2014).
43. F. M. Lambers, A. R. Bouman, C. M. Rimnac, C. J. Hernandez, Microdamage caused by fatigue loading in human cancellous bone: relationship to reductions in bone biomechanical performance. *PLoS One* **8**, e83662 (2013).
44. F. Cosman, D. B. Crittenden, J. D. Adachi, N. Binkley, E. Czerwinski, S. Ferrari, L. C. Hofbauer, E. Lau, E. M. Lewiecki, A. Miyauchi, C. A. Zerbini, C. E. Milmont, L. Chen, J. Maddox, P. D. Meisner, C. Libanati, A. Grauer, Romosozumab Treatment in Postmenopausal Women with Osteoporosis. *N Engl J Med* **375**, 1532-1543 (2016).
45. T. M. Keaveny, E. F. Wachtel, D. L. Kopperdahl, Mechanical behavior of human trabecular bone after overloading. *J Orthop Res* **17**, 346-353 (1999).
46. E. F. Eriksen, R. Chapurlat, R. W. Boyce, Y. Shi, J. P. Brown, S. Horlait, D. Betah, C. Libanati, P. Chavassieux, Modeling-Based Bone Formation After 2 Months of Romosozumab Treatment: Results From the FRAME Clinical Trial. *J Bone Miner Res* **37**, 36-40 (2022).
47. P. S. Hinton, P. Nigh, J. Thyfault, Serum sclerostin decreases following 12 months of resistance- or jump-training in men with low bone mass. *Bone* **96**, 85-90 (2017).

48. K. Kerschan-Schindl, M. M. Thalmann, E. Weiss, M. Tsironi, U. Foger-Samwald, J. Meinhart, K. Skenderi, P. Pietschmann, Changes in Serum Levels of Myokines and Wnt-Antagonists after an Ultramarathon Race. *PLoS One* **10**, e0132478 (2015).
49. F. M. Lambers, G. Kuhn, F. A. Schulte, K. Koch, R. Muller, Longitudinal assessment of in vivo bone dynamics in a mouse tail model of postmenopausal osteoporosis. *Calcif Tissue Int* **90**, 108-119 (2012).
50. D. J. Webster, P. L. Morley, G. H. van Lenthe, R. Muller, A novel in vivo mouse model for mechanically stimulated bone adaptation--a combined experimental and computational validation study. *Comput Methods Biomech Biomed Engin* **11**, 435-441 (2008).
51. A. C. Scheuren, P. Vallaster, G. A. Kuhn, G. R. Paul, A. Malhotra, Y. Kameo, R. Muller, Mechano-Regulation of Trabecular Bone Adaptation Is Controlled by the Local in vivo Environment and Logarithmically Dependent on Loading Frequency. *Front Bioeng Biotechnol* **8**, 566346 (2020).
52. M. L. Bouxsein, S. K. Boyd, B. A. Christiansen, R. E. Guldberg, K. J. Jepsen, R. Müller, Guidelines for Assessment of Bone Microstructure in Rodents Using Micro-Computed Tomography. *Journal of Bone and Mineral Research* **25**, 1468-1486 (2010).
53. F. A. Schulte, F. M. Lambers, G. Kuhn, R. Muller, In vivo micro-computed tomography allows direct three-dimensional quantification of both bone formation and bone resorption parameters using time-lapsed imaging. *Bone* **48**, 433-442 (2011).
54. C. Flaig, P. Arbenz, A scalable memory efficient multigrid solver for micro-finite element analyses based on CT images. *Parallel Comput* **37**, 846-854 (2011).
55. P. Christen, B. van Rietbergen, F. M. Lambers, R. Muller, K. Ito, Bone morphology allows estimation of loading history in a murine model of bone adaptation. *Biomech Model Mechanobiol* **11**, 483-492 (2012).
56. W. Pistoia, B. Van Rietbergen, E. M. Lochmüller, C. A. Lill, F. Eckstein, P. Rüegsegger, Estimation of distal radius failure load with micro-finite element analysis models based on three-dimensional peripheral quantitative computed tomography images. *Bone* **30**, 842-848 (2002).
57. A. C. Davison, D. V. Hinkley, E. Schechtman, Efficient Bootstrap Simulation. *Biometrika* **73**, 555-566 (1986).
58. R. D. C. Team, in *R Foundation for Statistical Computing*. (Vienna, Austria, 2007).